Investigation of the role of break-up processes on the fusion of ^{16}O induced reactions

Devendra P. Singh,[1,*] Unnati,[1] Pushpendra P. Singh,[1] Abhishek Yadav,[1] Manoj Kumar Sharma,[2] B. P. Singh,[1,†] K. S. Golda,[3] Rakesh Kumar,[3] A. K. Sinha,[4] and R. Prasad[1]

[1]*Department of Physics, Aligarh Muslim University, Aligarh (UP) 202 002, India*

[2]*Department of Physics, S. V. College, Aligarh (UP) 202 001, India*

[3]*Inter-University Accelerator Center, Aruna Asaf Ali Marg, New Delhi 110 067, India*

[4]*UGC-DAE-CSR, Bidhan Nagar, Kolkata 700 098, India*

(Received 27 March 2009; published 7 July 2009)

An experiment was carried out to explore heavy ion incomplete fusion reaction dynamics, within the framework of the break-up fusion model, at energies near and above the Coulomb barrier. Excitation functions for several radionuclides produced via xn, pxn, and αxn channels were measured in the $^{16}O + ^{181}Ta$ system at energies of ≈76–100 MeV. The experimental excitation functions were compared with those calculated using the theoretical model code PACE4. It was observed that excitation functions of xn/pxn channels are in good agreement with theoretical predictions. However, a significant enhancement in the measured excitation functions of α-emitting channels was observed and attributed to the incomplete fusion processes. The incomplete fusion fraction (F_{ICF}) that gives the relative importance of complete and incomplete fusion processes was found to increase with energy. The results are discussed in terms of α-cluster structure of the projectile on various fusion reactions.

DOI: 10.1103/PhysRevC.80.014601 PACS number(s): 25.70.Jj, 25.70.Gh

I. INTRODUCTION

For many years, the study of heavy ion (HI) induced reactions has been used as an important tool to understand the reaction dynamics and the decay characteristics of excited compound nuclei at energies near and above the Coulomb barrier (CB) [1–4]. It is now experimentally established that complete (CF) and incomplete fusion (ICF) are the most dominating modes of reaction processes at these energies [5–10]. In the case of CF, all the nucleons of the projectile and target nuclei lose their identity and form a single, excited complex system, which may eventually lead to a fully equilibrated compound nucleus (CN). The equilibrium state occurs as the composite system produces an intense mean field that prevents the escape of nucleons from the excited complex system and leads to complete thermalization. At later stages, the CN de-excites via emission of light nuclear particle(s) and/or the characteristic γ rays. However, in case of ICF, as the projectile comes within the field of the target nucleus, it is assumed to break up into its fragments (predominantly into α clusters, in the case of the projectiles having an α-cluster structure), where one of the fragments may get fused with the target nucleus leading to the formation of an excited incompletely fused composite (IFC) system with a mass and/or charge less than the CN formed via CF [7]. The unfused fragment flows in forward cone with almost projectile velocity. Further, it has also been observed that, apart from CF and ICF, pre-equilibrium (PE) emission of light nuclear particles may also take place at these energies before the thermalization of the composite system [11–15]. Recently, it has been observed that ICF becomes more and more dominant as the projectile energy increases [16–21]. The different modes of reactions can also be understood on the basis of driving input angular momenta imparted into the system. The CF occurs for the input angular momenta values $\leqslant l_{crit}$, as per the sharp cutoff approximation. However, at relatively higher projectile energies and/or at larger impact parameters, ICF starts influencing the CF. It may, further, be pointed out that the multitude of driving input angular momenta may vary with the projectile energy and/or with the impact parameter. However, there is no sharp boundary for the CF and ICF processes; both the processes have been observed below and/or above the limiting value of input angular momenta [22]. A few reports have indicated that ICF can selectively populate high spin states in the final reaction products at low bombarding energies and can be used as a spectroscopic tool as well [23,24]. The ICF reactions have been demonstrated to populate neutron-rich nuclei compared to conventional fusion-evaporation reactions, opening possibilities for the study of nuclei along the neutron-rich side of the line of stability [25].

A variety of dynamical models/theories, like the Break-up Fusion (BUF) model [26], the SUMRULE model [27], the Promptly Emitted Particles (PEPs) model [28], the EXCITON model [29], the Hot Spot model [30], the Multistep Direct Reaction theory [31], and the Overlap model [32–34], have been proposed to explain ICF dynamics. Apart from the aforementioned dynamical models, Mogenstern *et al.* [35,36] investigated the mass asymmetry dependence of the ICF contribution. The details of the above models are given in Ref. [20]. It may, however, be pointed out that these models correctly predict the magnitude of ICF, to some extent, in some cases at energies ⩾10 MeV/nucleon, but none of these models/theories is able to successfully explain the ICF data at energies of ≈4–7 MeV/nucleon. As such, the study of ICF is still an active area of investigation. Despite the existence of so many models, a clear picture of the mechanism of ICF is yet to emerge, particularly at relatively low bombarding energies, i.e., ≈4–7 MeV/nucleon, where the systematic study

*dpsingh19@gmail.com
†bpsinghamu@gmail.com

is available only for a few projectile-target combinations [5,20].

As such, for better understanding of ICF dynamics at low energies, excitation functions (EFs) for several radionuclides produced in the $^{16}O+^{181}Ta$ system ($Z_1.Z_2 = 584$) have been measured in the projectile energy range ≈76–100 MeV. It may be pointed out that, the charge multiplication $Z_1.Z_2$ for the system is much less than 1600 and, therefore, the fission probability in this case is quite low [37]. Cavinato *et al.* [1] have also studied the same projectile-target combination and measured the EFs for the production of some isotopes of Tl, Hg, Au, Pt, Ir, Os, and Re at energies of ≈69–126 MeV. However, they have limited themselves to discussing the data concerning fusion reactions only and have not made any comment about ICF even for those reaction channels where α particles are emitted. In the present work, cross sections have been measured for those residues that may be populated via ICF processes as well. In the work of Cavinato *et al.* [1], a part of the data is obtained using the thick target-catcher technique and a part from the angular distribution. In the present work, up to 100 MeV, the cross sections have been measured at eight different energies using the thick target-catcher technique. Further, as already mentioned, the cross sections for several reactions expected to be populated via CF and/or ICF processes have been measured. The data set from Ref. [1], in general, agree with the present work in the overlapping energy range. In the present work, the $^{189,191}Pt$ isotopes studied by Cavinato *et al.* [1] could not be detected because of long half-lives and low intensities of γ radiations. Also, the cross sections for ^{190}Hg could not be measured because the threshold for this reaction is above 100 MeV. Cavinato *et al.* [1] have not measured the cross sections for the individual reaction channels and have measured the cumulative cross sections for Hg and Pt isotopes. In addition to the work presented in Ref. [1], the cross sections for several Tl isotopes populated by xn channels ($^{194}Tl^g$, $^{194}Tl^m$, $^{193}Tl^g$, $^{193}Tl^m$, $^{192}Tl^g$, and $^{192}Tl^m$) have been measured in the present work, which could not be measured by Cavinato *et al.* [1]. In view of the above, the present work not only supplements the data of earlier work [1] but also provides a new cross-section database for several residues. Further, in the present work, an attempt has also been made to estimate the relative contribution of CF and ICF to study the influence of ICF on CF processes. This article is organized as follows: a brief description of the experimental procedure is given in Sec. II, comparison and analysis of the experimental data with the theoretical model predictions is presented in Sec. IIIalong with the results and their interpretation. The conclusions drawn from the present study are given in the last section.

II. EXPERIMENTAL PROCEDURE

The experiment was performed using an $^{16}O^{7+}$ beam delivered from the 15UD-Pelletron Accelerator at the Inter-University Accelerator Centre (IUAC), New Delhi, India. Targets of spectroscopically pure ^{181}Ta (≈99.99%) of thickness ≈1.5 mg/cm^2 were prepared at the target laboratory of IUAC, using the rolling technique. To trap the recoiling products produced via different reaction processes, Al catchers of appropriate thickness were placed after each target. The thickness of each target and catcher foil was separately measured by weighing and also by the α-transmission method. The α-transmission method is based on the measurement of the energy lost by 5.487 MeV α particles (obtained from standard ^{241}Am source) while passing through the target material. Irradiations were carried out in the General Purpose Scattering Chamber (GPSC), which has an in-vacuum transfer facility (ITF). The targets along with the Al catchers in the form of a stack were placed normal to the beam direction, so that the recoiling products could be trapped in the catcher foils and there would be no loss of activity. The experimental setup (target-catcher foil arrangement) was similar to that given in Ref. [20]. Three stacks, each of four foils, three foils, and one foil, respectively, were irradiated at energies of ≈100, 98, and 88 MeV to cover a wide energy range. Keeping in view the half-lives of interest, irradiations were carried out for ≈8–10 h for each stack. The Pelletron crew provided a constant beam current ≈50 nA throughout the irradiations. The beam flux was calculated using the total charge collected in the Faraday cup, which was placed behind the target-catcher foil assembly. The activities produced after irradiation were recorded using a precalibrated, High Purity Germanium (HPGe) detector of

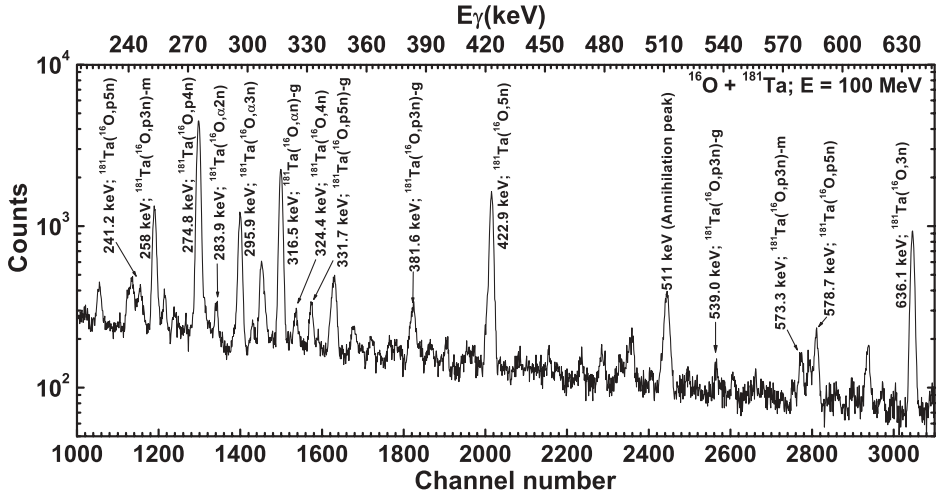

FIG. 1. An observed γ-ray spectrum of a ^{181}Ta sample irradiated by an ≈100 MeV $^{16}O^{7+}$ beam.

TABLE I. List of final reaction products along with populated channels and their spectroscopic properties.

Residue	$T_{1/2}$	J^{π}	E_{γ} (keV)	I_{γ} (%)
$^{194}Tl^{m}(3n)$	32.8 min	7^{+}	636.1	99
$^{194}Tl^{g}(3n)$	33 min	2^{-}	636.1	15.3
$^{193}Tl^{m}(4n)$	2.1min	$9/2^{-}$	365.0	90.1
$^{193}Tl^{g}(4n)$	21.6 min	$1/2^{+}$	324.4, 1044.7	15.2, 8.99
$^{192}Tl^{m}(5n)$	10.6 min	7^{+}	422.9	31.1
$^{192}Tl^{g}(5n)$	9.6 min	2^{-}	422.9	31.1
$^{193}Hg^{g}(p3n)$	3.8 h	$3/2^{-}$	381.6, 539.0	11.0, 1.2
			827.8, 861.1	4, 13.0
			1118.8	8.3
$^{193}Hg^{m}(p3n)$	11.8 h	$3/2^{-}$	258.1	60.0
$^{192}Hg(p4n)$	4.85 h	0^{+}	274.8	50.4
$^{191}Hg^{g}(p5n)$	49 min	$3/2^{-}$	224.6, 241.2	17.4, 8.9
			331.7	11.24
$^{191}Hg^{m}(p5n)$	50.8 min	$13/2^{+}$	420.3, 578.7	17.9, 17.0
$^{192}Au^{g}(\alpha n)$	4.94 h	1^{-}	295.5, 316.5	22.7, 58.0
$^{191}Au^{g}(\alpha 2n)$	3.18 h	$3/2^{+}$	283.9, 399.8	6.3, 4.5
$^{190}Au^{g}(\alpha 3n)$	42.8 min	1^{-}	295.9, 301.9	71.0, 25.1

100 c.c. active volume coupled to a PC through CAMAC based FREEDOM software [38]. The detector was calibrated using various standard γ sources, such as ^{60}Co, ^{133}Ba, and ^{152}Eu, of known strengths. The efficiency of the detector was determined at various source-detector separations. The detail of efficiency determination is given elsewhere [20].

A typical γ-ray spectrum for the $^{16}O + ^{181}Ta$ system at $\approx$100 MeV is shown in Fig. 1, where various γ peaks corresponding to different reaction products populated via CF and/or ICF channels are indicated. Further confirmation of the identification of reaction products has been made by the decay curve analysis. Identified evaporation residues along with their important spectroscopic properties are given in Table I. A FORTRAN programme based on standard formulation given in Ref. [20] has been used to determine the production cross sections of the reaction products. The experimentally measured cross sections for the population of residues via CF and/or ICF processes are given in Tables II and III. The errors in these measurements may arise mostly because of (a) nonuniformity of the target foil, (b) uncertainty in the determination of the efficiency of the detector, (c) fluctuations in the beam current, (d) the solid angle effect, etc. Details of errors due to above-mentioned factors are given in Ref. [20]. Attempts were made to minimize the uncertainties due to all the above factors. The overall error in the present work is estimated to be $\leqslant$15%, including the statistical errors.

III. RESULTS AND ANALYSIS OF DATA

To study the ICF reaction dynamics in the $^{16}O + ^{181}Ta$ system, the EFs for $^{194}Tl^{g}$, $^{194}Tl^{m}$, $^{193}Tl^{g}$, $^{193}Tl^{m}$, $^{192}Tl^{g}$, $^{192}Tl^{m}$, $^{193}Hg^{g}$, $^{193}Hg^{m}$, ^{192}Hg, $^{191}Hg^{g}$, $^{191}Hg^{m}$, $^{192}Au^{g}$, $^{191}Au^{g}$, and $^{190}Au^{g}$ radionuclides expected to be populated via CF and/or ICF were measured. A list of reactions populating various residues, their half-lives, characteristic γ lines, etc., is given in Table I. In general, a residue populated via a specific channel often emits several γ rays of different energies. The cross section for the channel was determined from the measured intensities of several characteristic γ rays and the value quoted is the weighted average of cross sections obtained for these γ rays [39].

A. (^{16}O, xn) channels

The measured EFs for residues populated via xn channels are shown in Fig. 2(a). Obviously these channels are populated only by CF. From the analysis of experimental data, activities corresponding to $3n$, $4n$, and $5n$ channels were identified. The identification was done on the basis of measured half-lives and γ-ray energies of the residues. It may be pointed out that in the case of $3n$ and $5n$ channels metastable and ground states of ^{194}Tl and ^{192}Tl are plotted. In both these cases, the metastable and ground states of the respective residues decay with γ rays of nearly the same energy and half-life. As such, the observed composite decay curves give the sum of both the states in each case. Individual cross sections were obtained by dividing the measured composite cross sections in the ratio of their γ-ray intensities [40,41]. $^{193}Tl^{g,m}$ are populated by a $4n$ channel. The metastable state of a half-life of $\approx$2 min decays to the ground state, which has a half-life of $\approx$22 min. Because counting of the irradiated samples was done after

TABLE II. Experimentally measured cross sections for the residues populated in the interaction of ^{16}O with the ^{181}Ta system.

Lab energy (MeV)	$\sigma(^{194}Tl^{m})$ (mb)	$\sigma(^{194}Tl^{g})$ (mb)	$\sigma(^{193}Tl^{m})$[a] (mb)	$\sigma(^{193}Tl^{g})$ (mb)	$\sigma(^{192}Tl^{m})$ (mb)	$\sigma(^{192}Tl^{g})$ (mb)	$\sigma(^{193}Hg^{g})$ (mb)	$\sigma(^{193}Hg^{m})$ (mb)
76 ± 1.1	2 ± 0.2	2 ± 0.2	0.1 ± 0.01	26 ± 3.8	–	–	23 ± 3.5	8 ± 0.8
80 ± 1.5	6 ± 0.8	6 ± 0.8	0.2 ± 0.02	45 ± 6.8	22 ± 3.2	22 ± 3.2	47 ± 7.0	21 ± 2.1
85 ± 1.2	4 ± 0.5	4 ± 0.5	0.3 ± 0.03	68 ± 10.2	61 ± 9.1	61 ± 9.1	60 ± 8.9	30 ± 3.0
87 ± 1.0	3 ± 0.4	3 ± 0.4	0.2 ± 0.02	46 ± 6.9	44 ± 6.5	44 ± 6.5	49 ± 7.4	22 ± 2.2
88 ± 1.6	2 ± 0.2	2 ± 0.2	0.2 ± 0.02	44 ± 6.5	91 ± 13.7	91 ± 13.7	42 ± 6.2	24 ± 2.3
93 ± 1.1	2.5 ± 0.3	2 ± 0.3	0.1 ± 0.01	35 ± 5.2	184 ± 27.6	184 ± 27.6	29 ± 4.4	13 ± 1.3
97 ± 1.0	2 ± 0.3	1.5 ± 0.2	0.1 ± 0.01	15 ± 2.3	171 ± 25.5	171 ± 25.5	12 ± 1.7	8 ± 0.7
99 ± 0.9	1 ± 0.1	1 ± 0.1	0.1 ± 0.01	17 ± 2.5	222 ± 33.3	222 ± 33.3	10 ± 1.5	6 ± 0.5

[a]Cross-section values give an upper limit.

TABLE III. Experimentally measured cross sections for the residues populated in the interaction of ^{16}O with the ^{181}Ta system.

Lab energy (MeV)	$\sigma(^{192}\mathrm{Hg})$ (mb)	$\sigma(^{191}\mathrm{Hg}^{g})$ (mb)	$\sigma(^{191}\mathrm{Hg}^{m})$ (mb)	$\sigma(^{192}\mathrm{Au}^{g})$ (mb)	$\sigma(^{191}\mathrm{Au}^{g})$ (mb)	$\sigma(^{190}\mathrm{Au}^{g})$ (mb)
80 ± 1.5	4 ± 0.5	–	–	2 ± 0.2	–	–
85 ± 1.2	40 ± 6.0	–	–	10 ± 1.5	–	8 ± 1.3
87 ± 1.0	36 ± 5.5	–	–	12 ± 1.8	2 ± 0.3	6 ± 0.8
88 ± 1.6	65 ± 9.8	3 ± 0.5	0.3 ± 0.04	31 ± 4.6	2 ± 0.3	23 ± 3.5
93 ± 1.1	121 ± 18.2	5 ± 0.7	3 ± 0.5	46 ± 6.9	3 ± 0.5	20 ± 2.9
97 ± 1.0	131 ± 6	$7 \pm .9$	8 ± 1.2	63 ± 9.5	14 ± 2.1	40 ± 5.9
99 ± 0.9	154 ± 23.2	14 ± 2.1	18 ± 2.7	50 ± 7.5	22 ± 3.2	21 ± 3.2

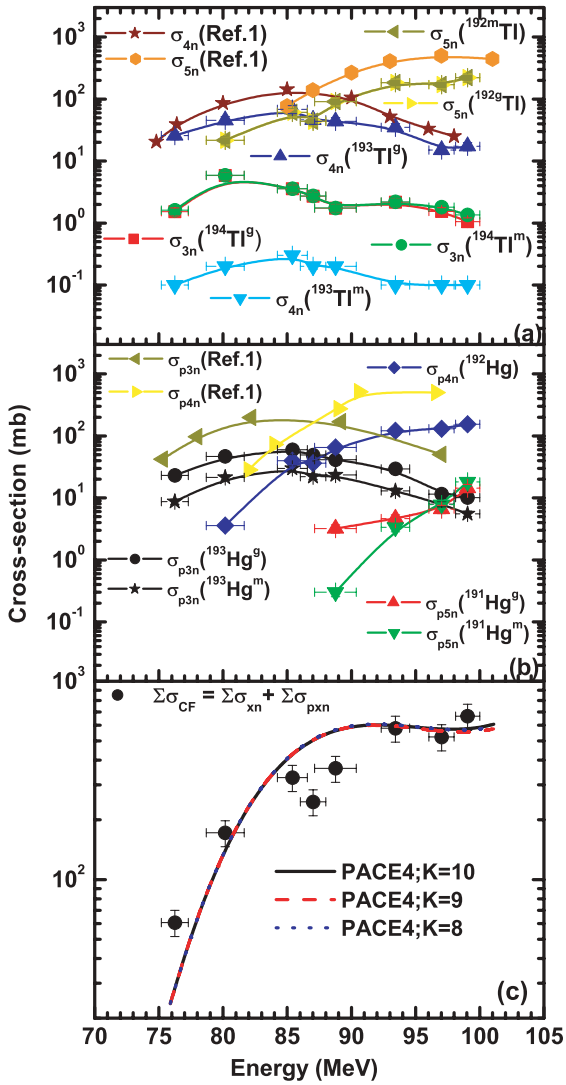

FIG. 2. (Color online) Measured EFs for (a) xn ($x = 3, 4$, and 5) channels and (b) pxn ($x = 3, 4$, and 5) channels. In panels (a) and (b), the spline-like lines joining the experimental data points are just to guide the eyes. Panel (c) shows the sum of cross sections for the xn and pxn channels. The effect of the variation of the choice of the level density parameter $K = 8, 9$, and 10 (dotted, dashed, and solid lines, respectively) on calculated $\Sigma\sigma_{\mathrm{CF}}$ is also shown.

about 10 min from the cessation of irradiation, the measured cross sections for the ground state also contain contributions ($\leqslant 0.38\%$) from the metastable state. As such, an upper limit for the cross section for the independent production of the metastable state has been determined and is given in Table II. The sum of cross sections ($\Sigma\sigma_{xn}$) for all the populated residues produced via xn ($x = 3, 4$, and 5) channels is also shown in Fig. 2(a), indicating the initial rise in $\Sigma\sigma_{xn}$ values and then nearly saturating at higher energies.

B. (^{16}O, pxn) channels

In the case of pxn channels, there is no likelihood of ICF and, therefore, these channels are also populated by CF only like xn channels. Residues corresponding to $p3n$, $p4n$, and $p5n$ channels have been identified through their characteristic γ rays and also by the respective half-lives. In the case of the $p3n$ and $p5n$ channels metastable and ground states of the residues are populated while in the case of the $p4n$ channel only one state is formed. All the residues in the pxn cases decay independently with their respective half-lives and γ rays of known energies. The cross sections for these channels are plotted in Fig. 2(b) and are tabulated in Tables II and III. Note that in the case of pxn channels the residues may be populated both by independent formation and also by the decay of the higher charge isobar precursor as shown below:

$$^{16}\mathrm{O} + {}^{181}\mathrm{Ta} \Longrightarrow {}^{197}\mathrm{Tl}^{*} \Longrightarrow {}^{193}\mathrm{Tl}^{*} + 4n;$$
$$^{193}\mathrm{Tl}^{*} \Longrightarrow {}^{193}\mathrm{Hg} + \beta^{+}/EC;$$
(precursor decay)
$$^{16}\mathrm{O} + {}^{181}\mathrm{Ta} \Longrightarrow {}^{197}\mathrm{Tl}^{*} \Longrightarrow {}^{193}\mathrm{Hg} + p3n.$$
(independent decay)

Similarly, the population of residues ^{192}Hg and ^{191}Hg may also be expected via the independent decay as well as the precursor decay of the type:

$$^{16}\mathrm{O} + {}^{181}\mathrm{Ta} \Longrightarrow {}^{197}\mathrm{Tl}^{*} \Longrightarrow {}^{192}\mathrm{Tl}^{*} + 5n;$$
$$^{192}\mathrm{Tl}^{*} \Longrightarrow {}^{192}\mathrm{Hg} + \beta^{+}/EC;$$
(precursor decay)
$$^{16}\mathrm{O} + {}^{181}\mathrm{Ta} \Longrightarrow {}^{197}\mathrm{Tl}^{*} \Longrightarrow {}^{192}\mathrm{Hg} + p4n;$$
(independent decay)

and

$$^{16}\mathrm{O} + {}^{181}\mathrm{Ta} \Longrightarrow {}^{197}\mathrm{Tl}^* \Longrightarrow {}^{191}\mathrm{Tl}^* + 6n;$$
$$^{191}\mathrm{Tl}^* \Longrightarrow {}^{191}\mathrm{Hg} + \beta^+/EC;$$
(precursor decay)
$$^{16}\mathrm{O} + {}^{181}\mathrm{Ta} \Longrightarrow {}^{197}\mathrm{Tl}^* \Longrightarrow {}^{191}\mathrm{Hg} + p5n.$$
(independent decay)

However, in the case of the $p5n$ channel, the precursor ^{191}Tl, which may be produced by a $6n$ channel, is not likely to be produced in the present experiment on account of its higher threshold ($\geqslant$100 MeV). In the case of $p3n$ and $p4n$ channels, the contribution of precursor decay could not be determined because of either the incomplete decay or the unknown decay characteristics of the precursor. For example, in the case of the $p4n$ channel, the cross sections for the independent decay of precursor formed by the $5n$ channel determined from its characteristic γ rays are found to be higher than the cross sections for residue ^{192}Hg populated by the $p4n$ channel. This may happen, if the precursor does not feed the residue ^{192}Hg formed by the $p4n$ channel. As such, the decay scheme of ^{192}Hg and ^{193}Hg needs further investigation. The cross-section values quoted in Tables II and III for these reactions also contain precursor contribution, if any, in the case of $p3n$ and $p4n$ channels.

In Fig. 2(b), the sum of cross sections for all measured pxn channels, denoted by $\Sigma\sigma_{pxn}$, has been obtained by adding the measured cross sections for $p3n$, $p4n$, and $p5n$ channels. To determine the total measured fusion cross section $\Sigma\sigma_{\mathrm{CF}}$ (expt), the sum of cross sections due to xn channels, i.e., $\Sigma\sigma_{xn}$, and the sum of cross sections due to all measured pxn channels, i.e., $\Sigma\sigma_{pxn}$, have been added. The total $\Sigma\sigma_{\mathrm{CF}}$ (expt) shown in Fig. 2(c) has been compared with $\Sigma\sigma_{\mathrm{CF}}$ (Th) obtained using the code PACE4 [42] with different values of level density parameters a ($a = A/K$). This code is based on statistical Hausher Fashback formalism followed by Monte Carlo simulations to determine the decay sequence of an excited compound nucleus. The code calculates the cross sections for a particular reaction using Bass formulation [43]. A detailed discussion of this code is given in one of our recent works [20]. However, for the sake of completeness, it must be pointed out that nuclear level density plays a central role in any statistical analysis of nuclear reactions. In this code the most sensitive parameter is the level density parameter (LDP) a ($a = A/K$), which mainly governs the equilibrium state. Here, A is the atomic mass number of the compound nucleus and K is a free parameter. The value of K may be varied to match the experimental data. As can be seen from Fig. 2(c), the $\Sigma\sigma_{\mathrm{CF}}$ (expt) is in good agreement with theoretical $\Sigma\sigma_{\mathrm{CF}}$ values. The fact that the measured fusion cross section $\Sigma\sigma_{\mathrm{CF}}$ (expt) could be reproduced satisfactorily by PACE4 predictions strengthens the confidence in the choice of input parameters. Also, a value of LDP ($a = A/8$ MeV^{-1}) has also been suggested by Cavinato *et al.* [1] for nuclei far from the magic region. Further, the literature values [1] for fusion cross sections are found to agree well with the present measurements and are shown in Fig. 2(c).

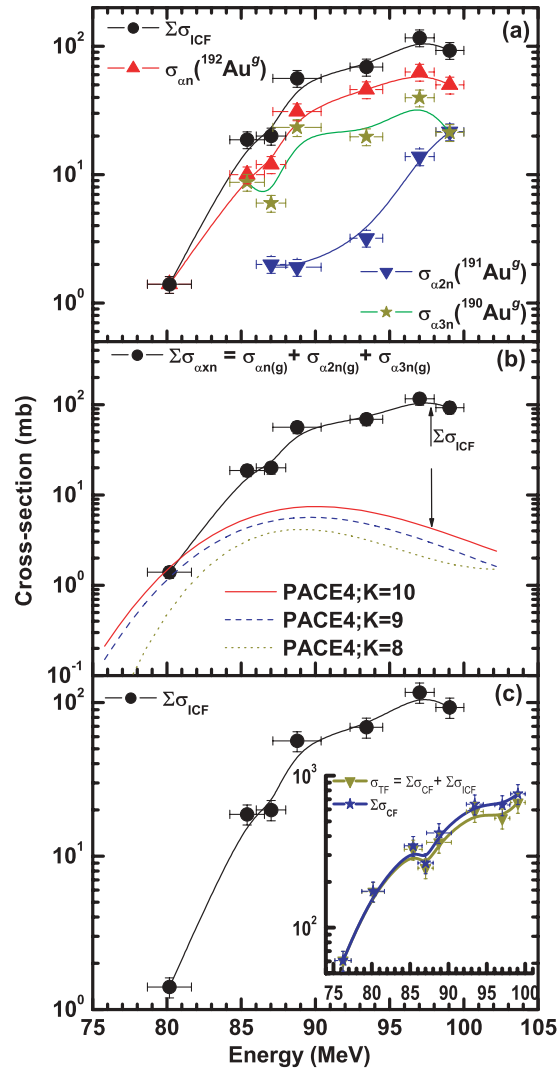

FIG. 3. (Color online) (a) Measured EFs for αxn ($x = 1, 2$, and 3) channels, (b) sum of the αxn channels, measured as well as calculated using PACE4 for $K = 8, 9, 10$ (dotted, dashed, and solid lines, respectively), and (c) sum of σ_{ICF} (all αxn) channels. In panels (a), (b), and (c), the spline-like lines joining the experimental data points are just to guide the eyes. The inset shows cross sections for the sum of both CF and ICF channels and for CF channels separately. The increasing difference, between the two curves in the inset, with energy indicates the dominance of ICF processes with energy.

C. (^{16}O, αxn) channels

In Fig. 3(a), the measured cross sections for the population of $^{193-x}$Au ($x = 1, 2$, and 3) isotopes via αxn channels are shown. Note that in the case of αxn channels, the residue may be formed in two ways: (i) by CF of ^{16}O followed by the formation of an excited CN from which evaporation of neutrons and α particles takes place, or (ii) the ^{16}O ion breaks into $\alpha + {}^{12}$C and ^{12}C fuses with the target leaving an α particle as a spectator. In this case the excited nucleus formed by the fusion of ^{12}C may emit neutrons while de-exciting. Option (i) refers to CF and option (ii) to ICF. These modes may be

represented by the following equations.

$$^{16}\mathrm{O}(^{12}\mathrm{C}+\alpha) \Longrightarrow {}^{12}\mathrm{C}+{}^{181}\mathrm{Ta} \Longrightarrow {}^{193}\mathrm{Au}^{*}+\alpha.$$

(α as spectator)

The residue $^{192}\mathrm{Au}^{g}$ may be populated via CF and/or ICF channels as

(i) complete fusion of ^{16}O, i.e.,

$$^{16}\mathrm{O}+{}^{181}\mathrm{Ta} \Longrightarrow {}^{197}\mathrm{Tl}^{*} \Longrightarrow {}^{192}\mathrm{Au}^{g*}+\alpha+n,$$

(ii) incomplete fusion of ^{16}O, i.e.,

$$^{16}\mathrm{O}(^{12}\mathrm{C}+\alpha)+{}^{181}\mathrm{Ta} \Longrightarrow {}^{193}\mathrm{Au}^{*}+\alpha,$$

(spectator)

$$^{193}\mathrm{Au}^{*} \Longrightarrow {}^{192}\mathrm{Au}^{g*}+n.$$

The residue $^{191}\mathrm{Au}^{g}$ may be populated via CF and/or ICF channels as

(i) complete fusion of ^{16}O, i.e.,

$$^{16}\mathrm{O}+{}^{181}\mathrm{Ta} \Longrightarrow {}^{197}\mathrm{Tl}^{*} \Longrightarrow {}^{191}\mathrm{Au}^{g*}+\alpha+2n,$$

(ii) incomplete fusion of ^{16}O, i.e.,

$$^{16}\mathrm{O}(^{12}\mathrm{C}+\alpha)+{}^{181}\mathrm{Ta} \Longrightarrow {}^{193}\mathrm{Au}^{*}+\alpha,$$

(spectator)

$$^{193}\mathrm{Au}^{*} \Longrightarrow {}^{191}\mathrm{Au}^{g*}+2n.$$

Similarly, the residue $^{190}\mathrm{Au}^{g}$ may be populated via CF and/or ICF channels as

(i) complete fusion of ^{16}O, i.e.,

$$^{16}\mathrm{O}+{}^{181}\mathrm{Ta} \Longrightarrow {}^{197}\mathrm{Tl}^{*} \Longrightarrow {}^{190}\mathrm{Au}^{g*}+\alpha+3n,$$

(ii) incomplete fusion of ^{16}O, i.e.,

$$^{16}\mathrm{O}(^{12}\mathrm{C}+\alpha)+{}^{181}\mathrm{Ta} \Longrightarrow {}^{193}\mathrm{Au}^{*}+\alpha,$$

(spectator)

$$^{193}\mathrm{Au}^{*} \Longrightarrow {}^{190}\mathrm{Au}^{g*}+3n.$$

The residue $^{192}\mathrm{Au}^{g}$ may also be populated via the decay of ^{192}Hg via β^{+}/EC decay. Both, $^{192}\mathrm{Au}^{g}$ ($T_{1/2}=4.94$ h) and ^{192}Hg ($T_{1/2}=4.85$ h) have nearly the same half-lives. In this case, it has been possible to separate out the contribution from the decay of ^{192}Hg populated via the $p4n$ channel using decay analysis. It is known from the successive radioactive decay, if the daughter nucleus half-life (T_A) and the parent nucleus half-life (T_B) are nearly equal, as in the present case, such that $T_A = T_B(1+\delta)$, where $\delta \ll 1$, then the activity ratio increases approximately linearly with time, so long as $t \ll 2\tau_B/\delta$ [44], where τ_B is the mean lifetime of the parent nucleus. To obtain the cross section of $^{192}\mathrm{Au}^{g}$, a curve between the lapse time and its production cross section was plotted at different times and also at different energies. To obtain the independent cross sections at each energy, plots for different lapse times were extrapolated at $t=0$ time using a least-square linear fitting method. The cross section at time $t=0$ is the independent cross section for the production of $^{192}\mathrm{Au}^{g}$. In Fig. 3(a), the cross sections deduced as mentioned above for the independent production of $^{192}\mathrm{Au}^{g}$ have been plotted. Here [Fig. 3(a)] the sum of cross sections for all measured αxn channels, i.e., $\Sigma\sigma_{\alpha xn}$(expt), is also shown and is found to increase with energy. It has already been mentioned that all the α-emission channels identified in the present work are expected to have significant contributions from ICF processes. To determine the contribution from ICF processes to the αxn channels, the measured $\Sigma\sigma_{\alpha xn}$(expt) has been compared with the corresponding values calculated using the theoretical model code PACE4, which is based on statistical CN theory. Because the code does not take ICF into consideration, the calculated cross sections for $\Sigma\sigma_{\alpha xn}$ with code PACE4 have predictions based on the CF model only. In Fig. 3(b) a comparison of $\Sigma\sigma_{\alpha xn}$(expt) has been made with $\Sigma\sigma_{\alpha xn}$(Th) calculated theoretically using the CF model for three different values of physically acceptable [45] level density parameters ($K=8, 9,$ and 10). As can be seen from this figure, the $\Sigma\sigma_{\alpha xn}$(Th), with any of the reasonable parameters could not reproduce $\Sigma\sigma_{\alpha xn}$(expt) above 85 MeV. The measured $\Sigma\sigma_{\alpha xn}$(expt) agree very well with $\Sigma\sigma_{\alpha xn}$(Th) at 80 MeV. However, above this data point all the measured cross sections are found to be much higher as compared to those of theoretical predictions based on the PACE4 model. The difference between the experimental and the theoretical values of $\Sigma\sigma_{\alpha xn}$ may be assigned to ICF and has been denoted by $\Sigma\sigma_{\mathrm{ICF}}$(expt). Further, the difference between $\Sigma\sigma_{\alpha xn}$(expt) and $\Sigma\sigma_{\alpha xn}$(Th) is found to increase with energy above 80 MeV, indicating the dominance of ICF processes at relatively higher energies, with maximum ICF contribution at the highest studied energy i.e., 100 MeV. Further, in Fig. 3(c) $\Sigma\sigma_{\mathrm{ICF}}$ obtained by subtracting $\Sigma\sigma_{\mathrm{ICF}}$(Th) ($K=10$) from measured $\Sigma\sigma_{\alpha xn}$ is been plotted as a function of energy. As can be seen from this figure, ICF production increases very rapidly with energy. In the inset of Fig. 3(c) $\Sigma\sigma_{\mathrm{TF}}$ (total sum of cross sections for all measured channels) and $\Sigma\sigma_{\mathrm{CF}}$ are compared. As can be seen from Fig. 3(c) (inset), with the increase in energy the difference between σ_{TF} and $\Sigma\sigma_{\mathrm{CF}}$ continues to increase, indicating the dominance of ICF at relatively higher energies. In a complementary experiment [46], recoil ranges for the same residues have been determined to get information about the degree of linear momentum transfer and the relative contribution of CF and ICF channels. The relative contribution of CF and ICF channels obtained from the complementary experiment agree with the present data within the experimental uncertainties.

At energies above the CB, where $E \gg V_0$, the classical formula of Weisskopf [47] for capture of charge particle by a nucleus is given by

$$\sigma_{\mathrm{CF}}(E) = \pi r_0^2(1 - V_0/E),$$

where, V_0 is the value of CB and E is the energy in center of mass system. As such, if σ_{CF} (Exp) is plotted against $1/E_{\mathrm{c.m.}}$, it should be a linear curve. The deduced $\Sigma\sigma_{\mathrm{CF}}$ values from $\Sigma\sigma_{xn} + \Sigma\sigma_{pxn} + \Sigma\sigma_{\alpha xn}$(Th) have been plotted as a function of $1/E_{\mathrm{c.m.}}$ in Fig. 4. A fit to the $\Sigma\sigma_{\mathrm{CF}}$ data points indicates a linear curve that cuts the x axis at the beam energy equal to CB. It may, however, be pointed out that a departure from linearity above CB may indicate the approach to and beginning of a quantal regime giving rise to subbarrier fusion. Further,

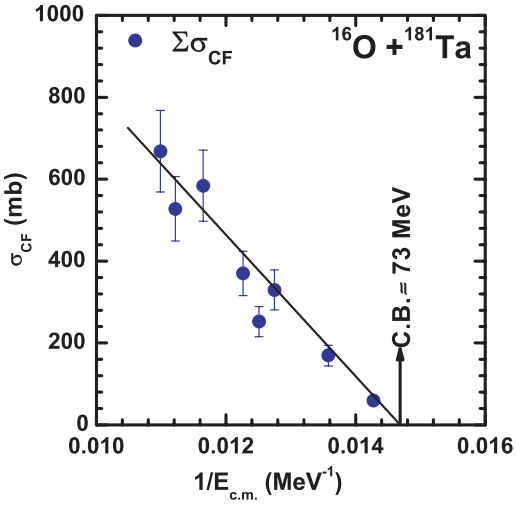

FIG. 4. (Color online) Experimentally measured production cross sections found to reproduce the Coulomb barrier of the system.

to study the dependence of ICF contribution on energy, for the presently studied system, the percentage fraction of ICF fusion cross section ($F_{\rm ICF}$) has been plotted in Fig. 5 as a function of beam energy normalized to CB, along with several other literature values [5,16,19,20]. As can be seen from this figure, $F_{\rm ICF}$ increases with the increase in normalized beam energy for all the systems. To study the dependence of $F_{\rm ICF}$ on mass asymmetry, the percent $F_{\rm ICF}$ has also been plotted in Fig. 6 as a function of mass asymmetry at a constant value ($E_{\rm beam}/V_b = 1.38$) of normalized beam energy. As can be seen from this figure, the $F_{\rm ICF}$ for the presently studied system is not following the expected trend shown for other systems involving ^{16}O beam. The present $F_{\rm ICF}$ for $^{16}\mathrm{O} + ^{181}\mathrm{Ta}$ is found to be significantly small. It may be because of the fact that in the present measurements several other α-emission channels, e.g., $2\alpha xn$ and $3\alpha xn$ channels, could not be observed as the

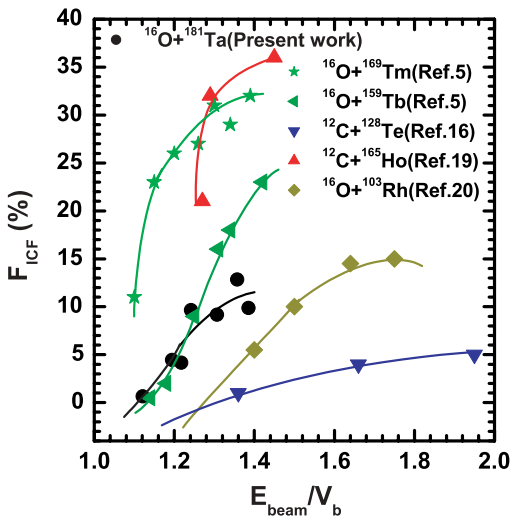

FIG. 5. (Color online) Deduced percentage ICF fraction ($F_{\rm ICF}$) as a function of normalized projectile energy for the $^{16}\mathrm{O} + ^{181}\mathrm{Ta}$ system along with literature values. The spline-like lines joining the experimental data points are just to guide the eyes.

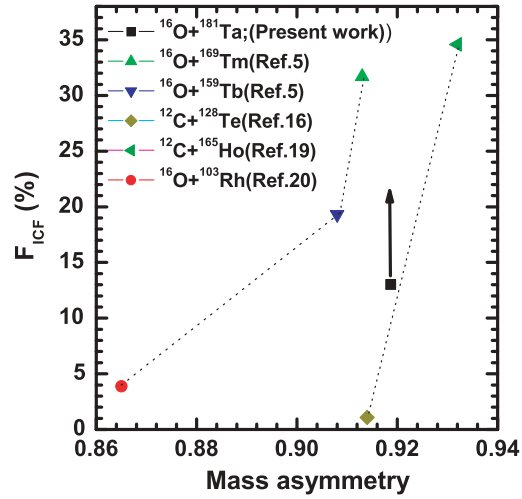

FIG. 6. (Color online) The percentage ICF fraction as a function of mass asymmetry at a constant normalized projectile energy. The arrow indicates that the present value of $F_{\rm ICF}$ for $^{16}\mathrm{O} + ^{181}\mathrm{Ta}$ is expected to go up, if all other remaining α-emission channels are also measured.

residues populated via these channels were either stable or short lived and/or had very low γ-ray intensity. We propose to measure the contribution of these α-emission channels in an in-beam experiment using particle-γ coincidence technique, so that the present data may be supplemented.

IV. CONCLUSIONS

In the present work, EFs for the production of 14 radionuclides, $^{194}\mathrm{Tl}^g(3n)$, $^{194}\mathrm{Tl}^m(3n)$, $^{193}\mathrm{Tl}^g(4n)$, $^{193}\mathrm{Tl}^m(4n)$, $^{192}\mathrm{Tl}^g(5n)$, $^{192}\mathrm{Tl}^m(5n)$, $^{193}\mathrm{Hg}^g(p3n)$, $^{193}\mathrm{Hg}^m(p3n)$, $^{192}\mathrm{Hg}(p4n)$, $^{191}\mathrm{Hg}^g(p5n)$, $^{191}\mathrm{Hg}^m(p5n)$, $^{192}\mathrm{Au}^g(\alpha n)$, $^{191}\mathrm{Au}^g(\alpha 2n)$, and $^{190}\mathrm{Au}^g(\alpha 3n)$, were measured. The experimental data were compared with the predictions of the theoretical code PACE4 based on a statistical model. The CF cross sections were found agree with PACE4 calculations over the entire energy range. A significant enhancement in the cross sections was observed, for α-emitting channels, as compared to the theoretical PACE4 model predictions. The observed enhancement was attributed to the prompt break up of the projectile into α clusters, with ^{16}O into $^{12}\mathrm{C} + ^{4}\mathrm{He}$ leading to the ICF process. As such, it may be concluded that apart from CF, ICF is also a process of greater importance even at these low energies and, hence, when predicting the total reaction cross sections, the ICF contribution should also be taken into consideration. Further, as expected $\Sigma\sigma_{\rm ICF}$ was found to increase with energy.

ACKNOWLEDGMENTS

The authors are thankful to Professor Amit Roy, Director, Inter-University Accelerator Centre (IUAC), New Delhi, India, for extending all the necessary facilities for performing the experiments and for extending hospitality. We are also thankful to Dr. R. K. Bhaumik for scientific discussions and support during the experiments. The authors also thank the Chairman,

Department of Physics, Aligarh Muslim University, Aligarh, for providing all the necessary facilities. One of the authors (DPS) thanks the UGC-DAE, Consortium for Scientific Research Calcutta Centre, India, for providing financial support under Project CRS-076/AMU/P/RP/7409, MKS thanks the DST, and RP thanks the DST and UGC.

[1] M. Cavinato, E. Fabrici, E. Gadioli, E. Gadioli Erba, P. Vergani, M. Crippa, G. Colombo, I. Redaelli, and M. Ripamonti, Phys. Rev. C **52**, 2577 (1995).
[2] P. Vergani, E. Gadioli, E. Vaciago, E. Fabrici, E. Gadioli Erba, M. Galmarini, G. Ciavola, and C. Marchetta, Phys. Rev. C **48**, 1815 (1993).
[3] F. Schussler, H. Nifenecker, B. Jakobsson, V. Kopljar, K. Soderstrom, S. Leray, C. Ngo, S. Souza, J. P. Bondrof, and K. Sneppen, Nucl. Phys. **A584**, 704 (1995).
[4] E. Gadioli, C. Brattari, M. Cavinato, E. Fabrici, E. Gadioli Erba, V. Allori, A. Di. Fillippo, S. Vailati, T. G. Stevens, S. H. Connell, J. P. F. Sellschop, F. M. Nortier, G. F. Steyn, and C. Marchetta, Nucl. Phys. **A641**, 271 (1998).
[5] P. P. Singh, B. P. Singh, M. K. Sharma, Unnati, D. P. Singh, R. Prasad, R. Kumar, and K. S. Golda, Phys. Rev. C **77**, 014607 (2008).
[6] P. P. Singh, M. K. Sharma, Unnati, D. P. Singh, R. Kumar, K. S. Golda, B. P. Singh, and R. Prasad, Eur. Phys. J. A **34**, 29 (2007).
[7] R. H. Siemsen *et al.*, Nucl. Phys. **A400**, 245c (1983).
[8] D. J. Parker, J. Asher, T. W. Conlon, and I. Naqib, Phys. Rev. C **30**, 143 (1984).
[9] Ch. Ngo, Prog. Part. Nucl. Phys. **16**, 139 (1985).
[10] D. R. Zolnowski, H. Yamada, S. E. Cala, A. C. Kahler, and T. T. Sugihara, Phys. Rev. Lett. **41**, 92 (1978).
[11] A. Yoshida *et al.*, Phys. Lett. **B44**, 1528 (1991).
[12] C. Signorini *et al.*, Nucl. Phys. **A735**, 329 (2004).
[13] M. Blann, Nucl. Phys. **A235**, 211 (1974).
[14] M. Blann, Annu. Rev. Nucl. Sci. **25**, 123 (1975).
[15] F. Amorini, M. Cabibbo, G. Cardelaa, A. Di Pietro, A. Musumarra, M. Papa, G. Pappalardo, F. Rizzo, and S. Tudisco, Phys. Rev. C **58**, 987 (1998).
[16] Manoj Kumar Sharma, B. P. Singh, Sunita Gupta, M. M. Muthafa, H. D. Bhardwaj, and R. Prasad, J. Phys. Soc. Jpn. **72**, 1917 (2003).
[17] M. K. Sharma, Unnati, B. K. Sharma, B. P. Singh, H. D. Bhardwaj, R. Kumar, K. S. Golda, and R. Prasad, Phys. Rev. C **70**, 044606 (2004).
[18] M. K. Sharma, Unnati, B. P. Singh, R. Kumar, K. S. Golda, H. D. Bhardwaj, and R. Prasad, Nucl. Phys. **A776**, 83 (2006).
[19] S. Gupta, B. P. Singh, M. M. Musthafa, H. D. Bhardwaj, and R. Prasad, Phys. Rev. C **61**, 064613 (2000).
[20] Unnati, P. P. Singh, D. P. Singh, M. K. Sharma, A. Yadav, R. Kumar, B. P. Singh, and R. Prasad, Nucl. Phys. **A811**, 77 (2008).
[21] P. P. Singh, B. P. Singh, M. K. Sharma, Unnati, R. Kumar, K. S. Golda, D. Singh, R. P. Singh, S. Muralithar, M. A. Ansari, R. Prasad, and R. K. Bhowmik, Phys. Rev. C **78**, 017602 (2008).
[22] I. Tserruya, V. Steiner, Z. Fraenkel, and P. Jacobs, Phys. Rev. Lett. **60**, 14 (1988).
[23] S. M. Mullins, A. P. Byrne, G. D. Dracoulis, T. R. McGoram, and W. A. Seale, Phys. Rev. C **58**, 831 (1998).
[24] S. M. Mullins, G. D. Dracoulis, A. P. Byrne, T. R. McGoram, S. Bayer, R. A. Bark, R. T. Newman, W. A. Seale, and F. G. Kondev, Phys. Rev. C **61**, 044315 (2000).
[25] G. J. Lane, G. D. Dracoulis, A. P. Byrne, A. R. Poletti, and T. R. McGoram, Phys. Rev. C **60**, 067301 (1999).
[26] T. Udagawa and T. Tamura, Phys. Rev. Lett. **45**, 1311 (1980).
[27] J. Wilczynski *et al.*, Phys. Rev. Lett. **45**, 606 (1980).
[28] J. P. Bondrof *et al.*, Nucl. Phys. **A333**, 285 (1980).
[29] M. Blann, Phys. Rev. Lett. **27**, 337 (1971).
[30] R. Weiner *et al.*, Nucl. Phys. **A286**, 282 (1977).
[31] V. I. Zagrebaev, Ann. Phys. (NY) **197**, 33 (1990).
[32] B. G. Harvey, Nucl. Phys. **A444**, 498 (1985).
[33] M. H. Simbel and A. Y. Abdul Magd, Z. Phys. A **294**, 277 (1980).
[34] A. Y. Abdul Magd, Z. Phys. A **298**, 143 (1980).
[35] H. Morgenstern, W. Bohne, W. Galster, D. G. Kovar, and H. Lehr, Phys. Lett. **B113**, 463 (1982).
[36] H. Morgenstern, W. Bohne, W. Galster, and K. Grabisch, Z. Phys. A **324**, 443 (1986).
[37] P. E. Hodgson, E. Gadioli, and E. Gadioli Erba, *Introductory Nuclear Physics* (Oxford University Press, London, 1997), Chap. 18.
[38] FREEDOM, data acquisition and analysis system designed to support the accelerator based experiments at the Nuclear Science Centre, New Delhi, India.
[39] S. F. Mughabghab, M. Divadeenam, and N. E. Holden, *Neutron Cross-Sections* (Academic Press, New York, 1981), Vol. 1, Part A, p. 89.
[40] E. Browne and R. B. Firestone, *Table of Radioactive Isotopes* (Wiley, New York, 1986).
[41] U. Reus and W. Westmeirer, At. Data Nucl. Data Tables **29**, 338 (1983).
[42] A. Gavron, Phys. Rev. C **21**, 230 (1980).
[43] R. Bass, Nucl. Phys. **A231**, 45 (1974).
[44] R. D. Evans, *The Atomic Nucleus* (McGraw–Hill, New York, 1982), p. 481.
[45] M. Blann, G. Reffo, and F. Fabbri, Nucl. Instrum. Methods A **265**, 490 (1988).
[46] Devendra P. Singh *et al.*, Ph.D. thesis, Aligarh Muslim University, Aligarh 202002, India (to be submitted, 2009).
[47] V. Weisskopf, Phys. Rev. **52**, 295 (1937).